Journal of The Electrochemical Society, **155** (6) H390-H395 (2008)
0013-4651/2008/155(6)/H390/6/$23.00 © The Electrochemical Society

Optical and Carrier Transport Properties of Cosputtered Zn–In–Sn–O Films and Their Applications to TFTs

Kachirayil J. Saji,[a] Madambi K. Jayaraj,[a,z] Kenji Nomura,[b] Toshio Kamiya,[b] and Hideo Hosono[b]

[a]*Optoelectronic Devices Laboratory, Department of Physics, Cochin University of Science and Technology, Kochi 682 022, India*
[b]*Materials and Structures Laboratory, Tokyo Institute of Technology, Midori-ku, Yokohama 226-8503, Japan*

The optical and carrier transport properties of amorphous transparent zinc indium tin oxide (ZITO)(a-ZITO) thin films and the characteristics of the thin-film transistors (TFTs) were examined as a function of chemical composition. The as-deposited films were very conductive and showed clear free carrier absorption (FCA). The analysis of the FCA gave the effective mass value of 0.53 m_e and a momentum relaxation time of 3.9 fs for an a-ZITO film with Zn:In:Sn = 0.35:0.35:0.3. TFTs with the as-deposited channels did not show current modulation due to the high carrier density in the channels. Thermal annealing at 300°C decreased the carrier density and TFTs fabricated with the annealed channels operated with positive threshold voltages (V_T) when Zn contents were 25 atom % or larger. V_T shifted to larger negative values, and subthreshold voltage swing increased with decreasing the Zn content, while large on–off current ratios 10^7–10^8 were kept for all the Zn contents. The field effect mobilities ranged from 12.4 to 3.4 $cm^2\ V^{-1}\ s^{-1}$ for the TFTs with Zn contents varying from 5 to 48 atom %. The role of Zn content is also discussed in relation to the carrier transport properties and amorphous structures.
 [DOI: 10.1149/1.2903866]

Manuscript submitted November 20, 2007; revised manuscript received February 18, 2008.
Available electronically April 14, 2008.

High-resolution and large-area flat panel displays (FPDs) require thin-film transistor (TFT) based active matrix driving schemes to suppress image blinking and to reduce power dissipation. TFT technology has been receiving more attention because it is also a promising means for achieving three-dimensional integration.[1] Amorphous semiconductors are preferred over polycrystalline ones for active layers in TFTs because of low processing temperature and high uniformity of device characteristics. In contrast to low mobility in covalent bonded amorphous materials (where carrier transport is controlled by hopping between localized tail states), degenerate band conduction and thereby high mobilities are possible in amorphous oxide semiconductors containing post-transition metal cations. The bottom of the conduction band in these oxide semiconductors having a high ionicity is primarily composed of spatially spread metal *ns* orbitals with isotropic shapes (*n* is the principal quantum number), and direct overlap among neighboring metal *ns* orbitals is possible.[2-5]

Several amorphous semiconductor materials like zinc oxide,[6] indium gallium zinc oxide,[7-12] zinc tin oxide,[13,14] gallium nitride,[15] and zinc indium oxide[16-19] have been employed as TFT n-channel layers in recent years. Grover et al. have reported the use of amorphous ZITO as channel ($ZnO:In_2O_3:SnO_2$ molar ratio 5:20:75) layers in depletion-mode TFTs.[20] These channel layer materials have excellent optical transmission in the visible region and the electrical conductivity can be controlled by adjusting the processing conditions.[21-25] As such, amorphous oxide semiconductors are promising materials for TFT technology, and there are plenty of works remaining to be surveyed to improve active layer materials with new chemical compositions. It is not easy to vary the film chemical composition by a conventional sputtering technique because one needs to prepare a ceramic target for each chemical composition.[9,25]

In the present work, we studied the optical and electron-transport properties of a ZITO system because there have been no systematic studies on the effects of chemical composition in ZITO films. We employed a cosputtering technique, because it is an effective technique for a multicomponent film to control the film chemical composition in a systematic and easy way. Our apparatus has both radio frequency (rf) sputtering and dc sputtering systems, enabling us to choose a process appropriate for the sputtering target. For the ZITO system, dc sputtering was employed for a conducting indium tin oxide target, because dc sputtering is a mass-production-compatible method which is actually used in FPD manufacturing and a faster growth method for a conducting target. RF sputtering was used for zinc oxide because we can use a high-resistivity powder as a target without a troublesome sintering process. The optoelectronic properties of amorphous and transparent ZITO films and the characteristics of their TFTs were examined as a function of chemical composition. It was found that the Hall mobility and electron concentration increased with increasing the Zn content for the as-deposited films, while the Tauc gap decreased.[26] Clear infrared absorptions due to free carrier absorptions (FCAs) were observed in optical absorption spectra, which are consistent with the large electron concentrations $>10^{20}\ cm^{-3}$. Due to the high electron concentrations, TFTs fabricated using the as-deposited films for the channels did not show source-to-drain current modulation. Thermal annealing of the TFTs at 300°C in air resulted in TFT operations for all the chemical compositions.

Experimental

The ZITO films were deposited by the dc-rf cosputtering technique to control the film chemical composition (Fig. 1). High-purity ZnO powder was used as the rf target, and presintered $In_2Sn_2O_7$ ceramic [a mixture of In_2O_3 and SnO_2, which was confirmed by X-ray diffraction (XRD)] was used as the dc target in a sputter-up configuration. Both targets were in a plane, and the substrate was rotated at a speed of 50 rpm at 4 cm above the targets. The dc power and current were fixed at 125 W and 200 mA, respectively (i.e., the sputtering rate of $In_2Sn_2O_7$ was fixed), while the rf power was varied from 25 to 200 W to vary the Zn content in the films. Argon pressure of 1 Pa was maintained in the chamber, and there was no intentional heating of the substrate during the deposition. Approximately 300 nm thick films were deposited on silica glass substrates for X-ray, optical, and Hall effect measurements. Thermally oxidized n-type Si wafers (sheet resistance is ~1 Ω) were used for substrates of TFTs. Some films were subjected to postdeposition thermal annealing at 300°C in air.

The chemical compositions of the films were measured by X-ray fluorescence (XRF) spectroscopy. The film structures were characterized by glancing-angle XRD at an incident angle of 0.5° using a Rigaku RINT-2000 with Cu Kα radiation. Carrier mobilities and concentrations were estimated by Hall measurements using the van der Pauw configuration. Optical reflectance (R) and transmission

[z] E-mail: mkj@cusat.ac.in

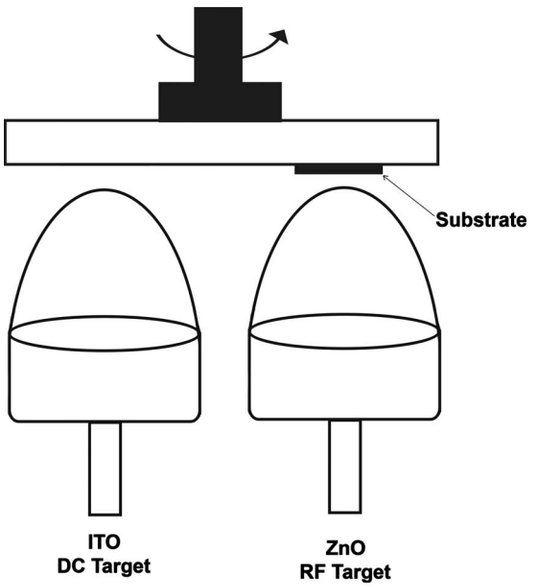

Figure 1. Schematic illustration of dc-rf cosputtering technique used for depositing the ZITO films. ZnO powders were used as the rf target and an $In_2Sn_2O_7$ ceramic as the dc target. Substrate was rotated at 50 rpm at 4 cm above the targets using a stepper motor.

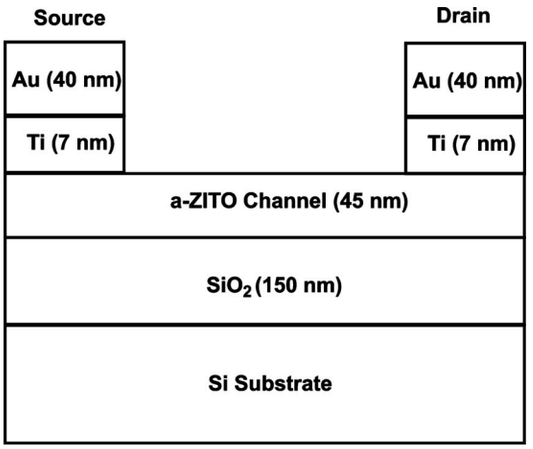

Figure 2. TFT structure using an amorphous layer of ZITO as a channel layer.

(T) spectra were measured using a near-infrared to UV double-beam spectrometer. Optical absorption coefficients (α) were calculated by correcting the reflection using a formula $e^{-\alpha d} = T/(1 - R)$, where d denotes the film thickness. The α-value of amorphous semiconductors generally follows a relationship of the form

$$\alpha h\nu = (\text{const})(h\nu - E_g)^r \quad [1]$$

where E_g is the optical bandgap (Tauc gap) and r is a constant. Using this model with $r = 2$ proposed by Tauc, E_g was estimated by linearly extrapolating the plot of $\sqrt{\alpha h\nu}$ vs $h\nu$ and finding the intersection with the abscissa (Tauc plot).[27,28] Effective mass and momentum relaxation time of free electrons were also analyzed from free carrier absorption spectra observed in high-conductivity as-deposited film by fitting an optical model to the observed R and T spectra. The optical model includes a film/glass substrate structure and a Caucy-type dispersion with a Drude-type free carrier absorption (details are reported in Ref. 29).

Bottom gate, top contact TFTs were fabricated using a-ZITO films with five different compositions for channels on the thermally oxidized n-type Si wafers. The thickness of the thermal oxide was 100 nm and that of the channels was ~45 nm. About 100 devices were fabricated in a 10×10 mm^2 area with a channel width and length of 300 and 50 μm, respectively, using lithography and lift-off. Ti/Au (7 nm/40 nm) stacks deposited by electron-beam evaporation were used as source and drain electrodes, while the thermal oxide and the Si substrate themselves act as a gate insulator and a gate electrode, respectively (device structure is shown in Fig. 2). Effects of post-thermal annealing were examined also for the TFTs. Some TFT chips were annealed at 300°C in air for 1 h after finishing the TFT fabrication process (i.e., annealed after depositing the Ti/Au electrodes). In addition, some TFTs were fabricated using channels annealed under the same condition before the Ti/Au deposition (i.e., the Ti/Au electrodes were deposited after the thermal annealing of the channels). Electrical characterizations of the TFTs were performed using a Keithley 4200 semiconductor characterization system.

Results and Discussion

Table I summarizes the chemical compositions measured by XRF and carrier transport properties obtained by Hall measurement for the films deposited on glass substrates with thicknesses of ~300 nm as a function of rf power applied to the ZnO target. It shows that the Zn content increases with the increase of rf power due to the increased sputtering rate of the ZnO target. The Sn/In composition ratios are nearly constant, ~0.8, because both Sn and In come from the same $In_2Sn_2O_7$ target, which indicates that we can take the Zn content as a control parameter to discuss the film properties and TFT characteristics. All the films were found to be amorphous, as observed by glancing-angle XRD (Fig. 3).

Table I also shows that the carrier concentration and mobility increase with the increase of Zn content, and the largest mobility of ~16 cm^2/Vs was obtained for the Zn:In:Sn = 0.5:0.27:0.23 film. All the films have very high electron concentrations $>5 \times 10^{19}$ cm^{-3}, because the sputtering was carried out in a reducing atmosphere (O_2-free Ar).

Despite the pure Ar plasma and high carrier concentrations, the films have high optical transmittance, larger than 90% in the visible region (Fig. 4a), while large optical absorptions are observed in the near-infrared region (1500–2500 nm). This IR absorption comes

Table I. Chemical composition and transport properties of a-ZITO films.

					As-prepared films		Annealed films	
RF power (W)	[Zn]	[In]	[Sn]	[Sn]/[In]	N_e (10^{20} cm^{-3})	μ (cm^2/V s)	N_e (10^{18} cm^{-3})	μ (cm^2/V s)
200	0.5	0.27	0.23	0.85	1.38	16.2	5.33	10.7
150	0.48	0.29	0.23	0.79	1.21	12.5	4.87	7.6
100	0.35	0.35	0.3	0.86	1.00	9.05	2.1	5.43
75	0.25	0.44	0.31	0.70	0.85	7.21	—	—
50	0.16	0.48	0.36	0.75	0.58	6.16	—	—
25	0.05	0.56	0.39	0.70	0.50	1.85	—	—

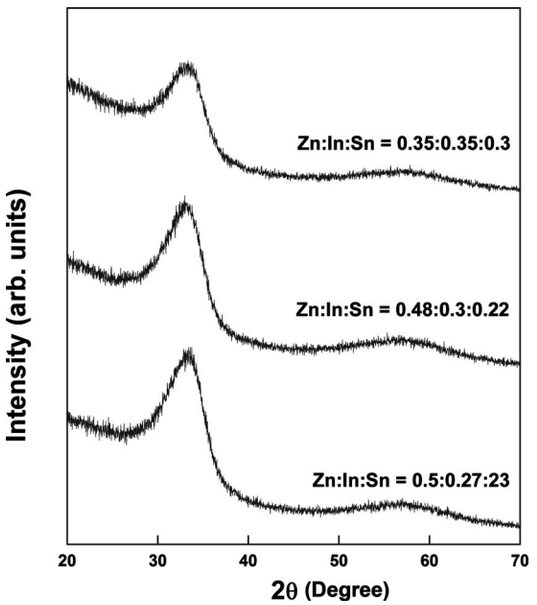

Figure 3. Glancing-angle XRD patterns of ZITO films deposited at different rf powers on glass substrates.

from reflection and absorption due to the free electrons (FCA) and is consistent with the high electron concentrations obtained by Hall measurement. We performed optical analyses for these data on the as-deposited films to extract an effective mass and a momentum relaxation time (τ) from FCA, but a reasonable fitting agreement to both the T and R spectra was obtained only for the Zn:In:Sn = 0.35:0.35:0.3 film. Figure 5 shows that the simulated T and R spectra agree well with the observed spectra, giving a plasma frequency of 0.51 eV and τ of 3.9 fs. Using the electron density obtained by the Hall measurement (1.0×10^{20} cm^{-3}), the effective mass of 0.53 m_e (m_e is the rest mass of electron) was obtained. It would be of interest to compare these results with another amorphous oxide semiconductor (AOS), a-InGaZnO$_4$. We reported the effective mass of 0.34 m_e and τ of 3.4 fs for an as-deposited

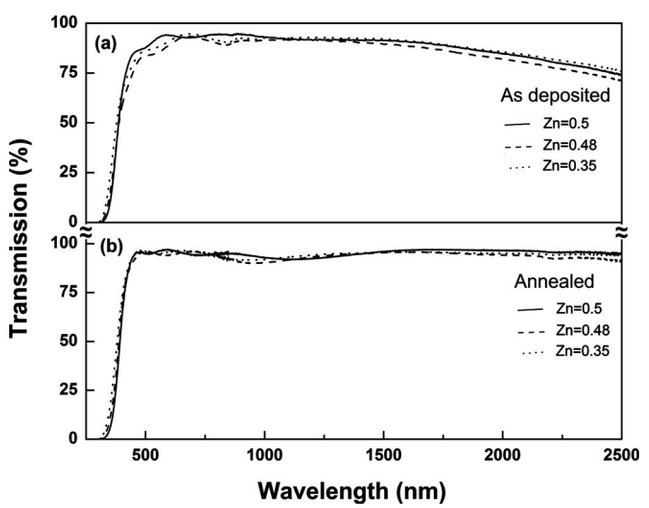

Figure 4. Optical transmission spectra through a-ZITO thin films (a) as-deposited and (b) annealed at 300°C having different Zn:In:Sn atomic ratios. The compositions Zn:In:Sn are (solid lines) 0.50:0.27:0.23, (dashed lines) 0.48:0.30:0.22, and (dotted lines) 0.35:0.35:0.30. Spectra are corrected for reflection. As-prepared films show large optical absorption in the IR region.

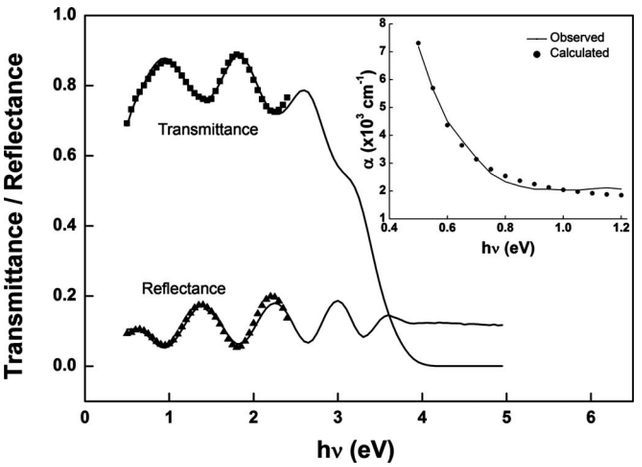

Figure 5. Fitting result of FCA analysis presented in transmittance (T) and reflectance (R) spectra for the Zn:In:Sn = 0.35:0.35:0.3 film. Solid lines: Observed R and T spectra. Symbols: Fitted results. Inset plots the observed and fitted results in optical absorption coefficients.

a-InGaZnO$_4$ film by fitting to only an optical absorption spectrum.[30] In this study, we employed a more reliable approach to use both the T and R spectra for the fitting procedures and obtained the effective mass of 0.36 m_e and τ of 4.4 fs for the as-deposited InGaZnO$_4$. Comparing these results indicates that the smaller mobility of the Zn:In:Sn = 0.35:0.35:0.3 film (9.1 cm^2/V s) than that of the latter a-InGaZnO$_4$ film (17 cm^2/V s) is primarily attributed to the heavier effective mass because the difference in τ is smaller than the difference in the effective masses.

The above results suggest that the a-ZITO films have large mobilities ~10 cm^2/V s and may produce high-mobility TFTs, but their carrier concentrations would be too high to effectively modulate the channel conductance by a gate bias voltage. Therefore we examined the effects of post-thermal annealing at 300°C in air. Figure 6a and b compares the optical absorption spectra before and after thermal annealing plotted in terms of the Tauc plot. It shows that the Tauc gaps of the as-prepared films decrease from 3.3 to 3.0 eV with increasing the Zn content from 0.35 to 0.50. Thermal annealing changed the Tauc gap from 3.30 to 3.20 eV for the Zn content of 0.35, for example. The slopes of the Tauc plots become sharper and the subgap absorptions beneath the Tauc gaps become smaller after thermal annealing. It is more clearly seen in the logarithmic plot (Fig. 6c and d). Thermal annealing caused the reduction of the extra absorptions in the vicinity of the Tauc gap. In the energy range $E < E_g$, the optical absorption coefficient shows a tail (Urbach tail) of the form $\alpha(h\nu) \propto \exp[(h\nu - E_g)/E_u]$, where E_u is the Urbach energy. The Urbach energies are estimated to be 0.20, 0.19, and 0.17 eV for the annealed films with Zn contents of 0.35, 0.48, and 0.5, respectively. The total area of subgap absorption decreases by thermal annealing. Hall measurements in Table I showed that the thermal annealing decreased the carrier concentrations drastically by 2 orders of magnitude to the order of 10^{18} cm^{-3}. The Hall mobilities were decreased at the same time, which is because the amorphous oxide semiconductors have a potential fluctuation around the conduction band minimum, and consequently, a large mobility is obtained at somewhat large carrier density which is enough to fill these potential valleys.[30] These results indicate that thermal annealing in air causes oxidation of the films and reduced the carrier concentration and the subgap states. TFTs were fabricated using ~45 nm thick, as-deposited a-ZITO channels, but those TFTs did not show any modulation in a source-to-drain current (I_{DS}) by a gate bias (V_G). This would be due to the large carrier concentrations in the channels. Then we annealed the TFTs (i.e., with the Ti/Au electrodes). Although the annealed TFTs showed TFT operations with

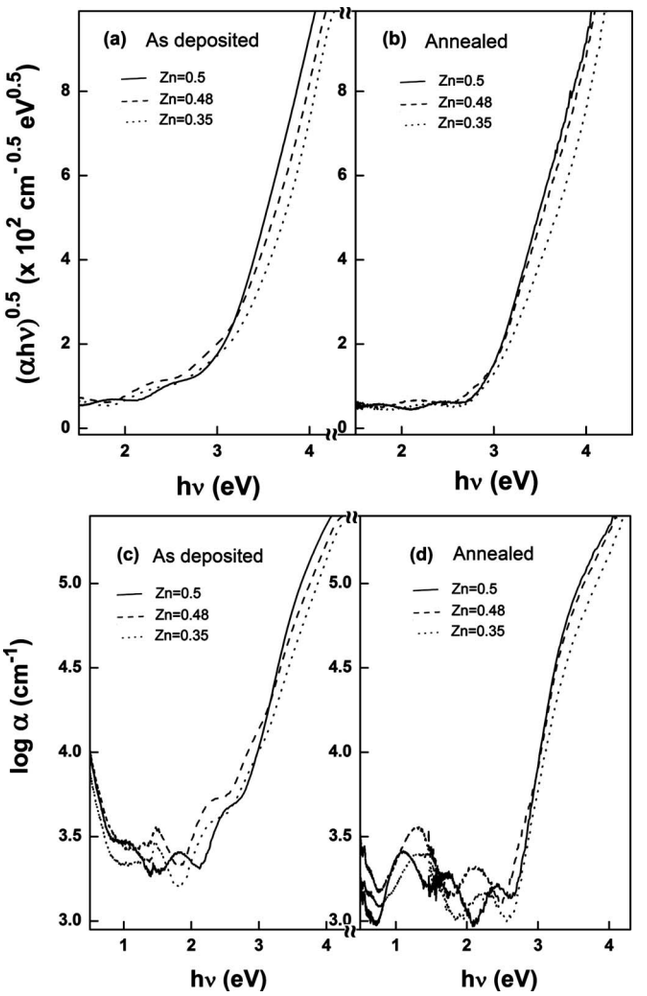

Figure 6. Tauc plots of (a) as-deposited and (b) annealed films as a function of Zn content. (c, d) Plots of log α–$h\nu$. The compositions Zn:In:Sn are (solid lines) 0.50:0.27:0.23, (dashed lines) 0.48:0.30:0.22, and (dotted lines) 0.35:0.35:0.30.

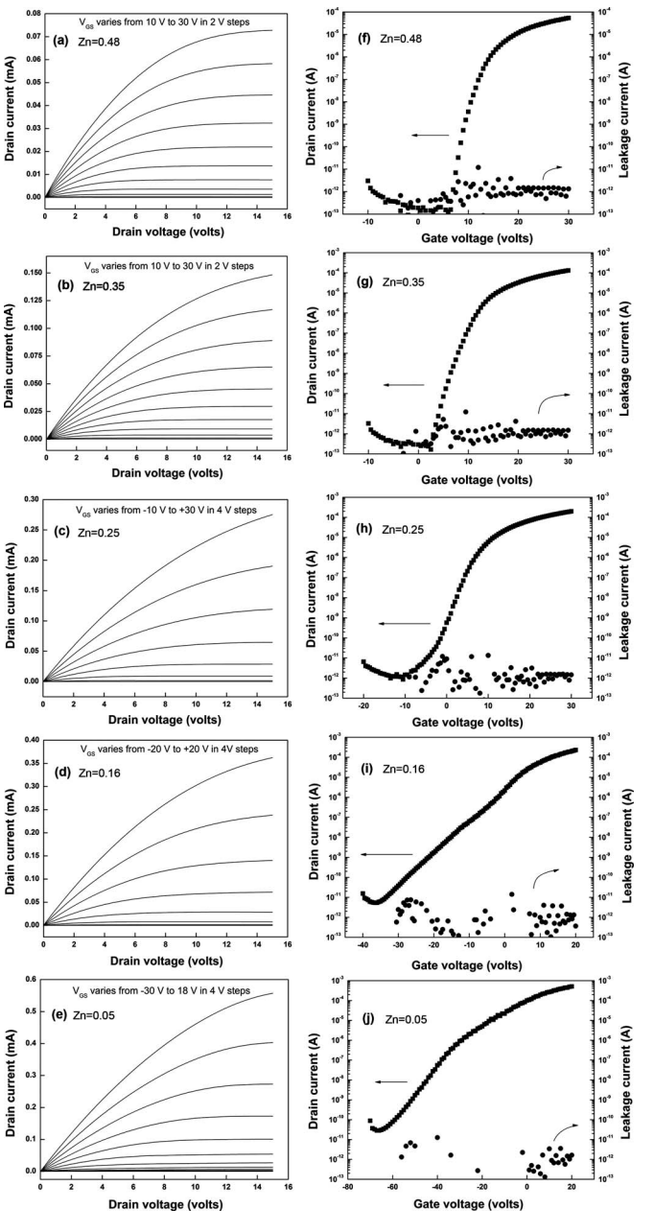

Figure 7. Output (I_{DS}–V_{DS}) and transfer [log(I_{DS})–V_G] characteristics of TFTs with different chemical compositions in the channel layer. (a–e) Output characteristics of a-ZITO channel TFTs with Zn:In:Sn atomic ratios 0.48:0.29:0.23, 0.35:0.35:0.30, 0.25:0.44:0.31, 0.16:0.48:0.36, and 0.05:0.56:0.39, respectively, and (f–j) shows corresponding transfer characteristics at V_{DS} = 10 V.

field effect mobilities of 10^{-2}–1 cm^2 V^{-1} s^{-1} and on–off current ratios of 10^4–10^5, their output characteristics showed nonideal characteristics with kinks, structures which are similar to those observed in simulation results considering acceptor-like states.[31] We speculated that these nonideal behaviors were caused by diffusion and/or oxidation of the Ti electrodes. Therefore, we annealed the a-ZITO channel/thermal oxide/Si samples before depositing Ti/Au electrodes and then formed the source-and-drain contacts to finish the TFT structures. Most of the TFTs operated with field effect mobilities varying from 3.4 to 12.4 cm^2 V^{-1} s^{-1} as the Zn content decreased from 48 to 5 atom %. Figure 7 summarizes the output and transfer characteristics of the TFTs. The I_{DS} values were very low, $<$0.1 nA in the off regions, and increased up to a few milliamperes by increasing V_G, indicating that the TFTs operated as n-channel transistors.

Transfer characteristics of the TFTs in Fig. 7 show on–off ratios of 10^7–10^8. Drain current in the nonsaturation region of the transistor operation is given by

$$I_{DS} = \frac{W\mu_{FE}C_i}{2L}[2(V_G - V_T)V_{DS} - V_{DS}^2] \quad [2]$$

where V_T is the threshold voltage, μ_{FE} is the field effect mobility, and C_i is the insulator capacitance per unit area. For a small constant value of V_{DS}, a plot of I_{DS} as a function of V_G would yield a straight line, the slope of which is proportional to μ_{FE}. By contrast, drain current in the saturation region (i.e., at V_{DS} greater than pinch-off voltage) is given by

$$I_{DS} = \frac{W\mu_{sat}C_i}{2L}(V_G - V_T)^2 \quad [3]$$

which provides the saturation mobility μ_{sat} and the threshold voltage V_T from a plot of $I_{DS}^{0.5}$ as a function of V_G.

For the TFT with the largest Zn content of 48 atom % (Fig. 7a and f, the μ_{FE} value, extracted from the slope of the linear region of the I_{DS}–V_G plot, was 3.4 cm^2/V s. Threshold voltage obtained by extrapolating a $I_{DS}^{0.5}$–V_G plot at V_{DS} = 10 V to the V_G axis was 12.1

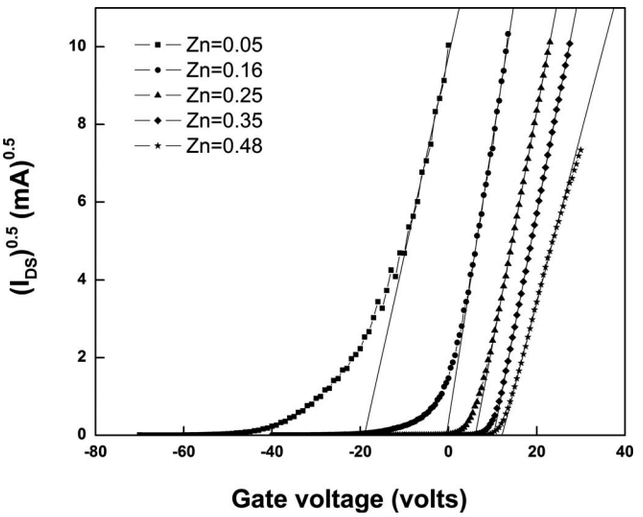

Figure 8. $(I_{DS})^{0.5}$ vs V_G plot for a-ZITO channel TFTs with different Zn:In:Sn atomic ratios at V_{DS} = 10 V. The channel Zn contents are shown in the figure. The slopes in the linear regions were used for extracting the saturation mobilities (μ_{sat}). Extrapolation of the linear region to the abscissa gives the threshold voltage (V_T).

V (Fig. 8). The positive threshold voltage indicates the enhancement mode operation of the device. Figure 7a exhibits hard saturation at large V_{DS}, which is similar to pinch-off in usual field-effect transistors. The TFTs using the other composition channels (Fig. 7b-e and g-j) showed similar output characteristics. The TFT with the smallest channel Zn content of 5 atom % showed significant current flow even at zero gate voltage. The soft saturation of drain current in the output characteristic indicates that the channel is not fully depleted, even if a large V_{DS} of 15 V was applied for $V_{GS} \leq 20$ V. Systematic variations were observed in the field-effect mobilities and V_T, where V_T increases with increasing Zn content. Variations in field effect mobility, saturation mobility, threshold voltage, subthreshold voltage swing (S), and current on–off ratio are tabulated in Table II. The TFT with the Zn content of 48 atom % operated in an enhanced mode with a V_T of 12.1 V, and that with 5 atom % operated in a depletion mode with a large negative V_T of −19 V. Subthreshold swing increased with decreasing the Zn content, indicating that the subgap trap densities increased with decreasing Zn content.

Finally, we mention the role of Zn ions with Zn content in a-ZITO films. Because we do not have enough experimental evidence, these are highly speculative, but it would be informative to try to understand the carrier transport properties obtained above. It was observed that the threshold voltage largely decreased and the S-value increased with decreasing Zn content. This trend is not specific to the a-ZITO system but is also observed in the a–In–Zn–O system.[9] The larger S-value indicates a larger density of subgap states (D_{it}), because the S-value is related to D_{it} by

$$S = \frac{2.3k_BT}{e}\left(1 + \frac{eD_{it}}{C_i}\right)$$

(C_i is the gate insulator capacitance).[32] Therefore, these experimental results suggest that the Zn-poor films have larger D_{it} and more donor states. This idea appears to contradict with the variation of carrier density, because Table I shows that the free carrier density derived by Hall measurements tends to decrease with decreasing Zn content. However, as it is also observed that the room-temperature Hall mobility largely decreases with decreasing Zn content, it is suggested that the Zn-poor films have more trap states, which decrease the free carrier concentration. This speculation is consistent with the TFT mobilities, because larger D_{it} decreases free carrier concentrations and channel conductance in the saturation regime of the TFTs, and consequently, the apparent μ_{sat} value is lower than drift mobility. The μ_{FE} value becomes larger for the Zn-poor films, probably because the μ_{FE} value is estimated above the subthreshold region from a differential of I_{DS} with respect to V_G and is less affected by D_{it}. Therefore, the μ_{FE} value more reflects drift mobility and carrier scattering in the channel. This means that the Zn-poor (i.e., In-rich) a-ZITO films have larger D_{it}, but extended drift mobilities would be larger, which is supported by Hall measurement on the a–In–Zn–O system in Ref. 5. The larger D_{it} in the Zn-poor films would be related to the local structure of multicomponent amorphous oxides. It is known that the structure of crystalline In_2O_3 is composed of an edge-sharing network of (InO_6) octahedra. This structure remains partly in amorphous $InGaZnO_4$,[33] and In–Zn–O,[34] and the portion of the edge-sharing structures decreases with decreasing In content, and the edge-sharing structures are converted to corner-sharing ones. As we pointed out in the amorphous Zn–Rh–O system,[35] an edge-sharing structure has a much stronger geometrical constraint to form an amorphous structure, and the increase in corner-sharing structures would form a more stable amorphous structure. We speculate that the increase in Zn content in a-ZITO films and probably also in other AOSs increases corner-sharing structures, forms a more stable amorphous structure, and reduces D_{it}. That is to say, Zn ions work as an effective stabilizer of amorphous structures in In_2O_3-based AOSs.[2]

Conclusion

a-ZITO thin films with different chemical compositions were deposited on glass substrates by cosputtering from ZnO and $In_2Sn_2O_7$ targets. Effects of postannealing on ZITO film properties and their TFT characteristics were analyzed. Electron Hall mobility increased with Zn content. The as-deposited films had high electron densities $\sim 10^{20}$ cm^{-3} and did not produce operating TFTs. The thermal annealing at 300°C reduced the electron densities to the order of 10^{18} cm^{-3} and produced operating TFTs. The TFT characteristics showed systematic variation with the chemical composition of the channels. The TFT having the largest Zn content 48 atom % showed a field effect mobility of ~3.4 cm^2/V s, a current on–off ratio of $\sim 10^8$, and a positive threshold voltage of ~12.1 V. The TFT having lowest Zn content 5 atom % showed a negative threshold voltage −19 V and a depletion mode operation. Cosputtering has been demonstrated as an effective technique for multicomponent oxide channel layer deposition. Although the present study demon-

Table II. Variations in TFT parameters with Zn content in the channel.

	TFT parameters				
RF power (W)	μ_{FE} (cm^2/V s)	μ_{sat} (cm^2/V s)	V_T (V)	S (V/dec)	On–off ratio
150	3.4	1.82	12.1	0.35	10^8
100	6.01	3.32	10.3	0.52	10^8
75	7.3	3.5	6.2	0.86	10^7
50	10.5	5.0	−0.6	2.65	10^7
25	12.4	2.9	−19	3.05	10^7

strated that ZITO channel TFTs operate even if the channels were deposited from powder ZnO targets, use of the powder target may limit the quality of the channels, and the TFT characteristics would be improved by using a higher quality target and further optimizing deposition conditions and channel chemical composition. Complete transparent ZITO transistors can be realized by using transparent substrates and gate oxide.

Acknowledgments

K.J.S. thanks the University Grants Commission, Government of India, for a research fellowship. M.K.J. thanks Tokyo Institute of Technology for the award of a visiting professorship. T.K. is supported by an Industrial Technology Research Grant Program (project ID: 06A12203d) in FY2006-2007 from the New Energy and Industrial Technology Development Organization (NEDO) of Japan.

References

1. D. J. Radack, in *Proceedings of the IEEE International SOI Conference*, IEEE, p. 5 (1999).
2. H. Hosono, N. Kikuchi, N. Ueda, and H. Kawazoe, *J. Non-Cryst. Solids*, **198–200**, 165 (1996).
3. H. Hosono, *J. Non-Cryst. Solids*, **352**, 851 (2006).
4. M. Orita, H. Ohta, M. Hirano, S. Narushima, and H. Hosono, *Philos. Mag. B*, **81**, 501 (2001).
5. K. Nomura, A. Takagi, T. Kamiya, H. Ohta, M. Hirano, and H. Hosono, *Jpn. J. Appl. Phys., Part 1*, **45**, 4303 (2006).
6. H. H. Hsieh and C. C. Wu, *Appl. Phys. Lett.*, **91**, 013502 (2007).
7. K. Nomura, H. Ohta, A. Takagi, T. Kamiya, M. Hirano, and H. Hosono, *Nature (London)*, **432**, 488 (2004).
8. H. Yabuta, M. Sano, K. Abe, T. Aiba, T. Den, H. Kumomi, K. Nomura, T. Kamiya, and H. Hosono, *Appl. Phys. Lett.*, **89**, 112123 (2006).
9. T. Iwasaki, N. Itagaki, T. Den, H. Kumomi, K. Nomura, T. Kamiya, and H. Hosono, *Appl. Phys. Lett.*, **90**, 242114 (2007).
10. M. Kim, J. H. Jeong, H. J. Lee, T. K. Ahn, H. S. Shin, J. S. Park, J. K. Jeong, Y. G. Mo, and H. D. Kim, *Appl. Phys. Lett.*, **90**, 212114 (2007).
11. D. Kang, H. Lim, C. Kim, I. Song, J. Park, Y. Park, and J. Chung, *Appl. Phys. Lett.*, **90**, 192101 (2007).
12. J. K. Jeong, J. H. Jeong, H. W. Yang, J. S. Park, Y. G. Mo, and H. D. Kim, *Appl. Phys. Lett.*, **91**, 113505 (2007).
13. H. Q. Chiang, J. F. Wager, R. L. Hoffman, J. Jeong, and D. A. Keszler, *Appl. Phys. Lett.*, **86**, 013503 (2005).
14. P. Görrn, P. Holzer, T. Riedl, W. Kowalsky, J. Wang, T. Weimann, P. Hinze, and S. Kipp, *Appl. Phys. Lett.*, **90**, 063502 (2007).
15. S. Kobayashi, S. Nonomura, T. Ohmori, K. Abe, S. Hirata, T. Uno, T. Gotoh, S. Nitta, and S. Kobayashi, *Appl. Surf. Sci.*, **113–114**, 480 (1997).
16. N. L. Dehuff, E. S. Kettenring, D. Hong, H. Q. Chiang, J. F. Wager, R. L. Hoffman, C. H. Park, and D. A. Keszler, *J. Appl. Phys.*, **97**, 064505 (2005).
17. P. Barquinha, P. Pimentel, A. Marques, L. Pereira, R. Martins, and E. Fortunato, *J. Non-Cryst. Solids*, **352**, 1756 (2006).
18. R. Martins, P. Barquinha, I. Ferreira, L. Pereira, G. Goncalves, and E. Fortunato, *J. Appl. Phys.*, **101**, 044505 (2007).
19. B. Yaglioglu, H. Y. Yeom, R. Bereshford, and D. C. Paine, *Appl. Phys. Lett.*, **89**, 062103 (2006).
20. M. S. Grover, P. A. Hersh, H. Q. Chiang, E. S. Kettenring, J. F. Wager, and D. A. Keszler, *J. Phys. D*, **40**, 1335 (2007).
21. T. Minami, H. Sonohara, T. Kakumu, and S. Takata, *Jpn. J. Appl. Phys., Part 2*, **34**, L971 (1995).
22. Y. S. Jung, Y. J. Seo, D. W. Lee, and D. Y. Jeon, *Thin Solid Films*, **445**, 63 (2003).
23. J. M. Phillips, R. J. Cava, G. A. Thomas, S. A. Carter, J. Kwo, T. Siegrist, J. J. Krajewski, J. H. Marshall, W. F. Peck, Jr., and D. H. Rapkine, *Appl. Phys. Lett.*, **67**, 2246 (1995).
24. T. Sasabayashi, N. Ito, E. Nishimura, M. Kon, P. K. Song, K. Utsumi, A. Kaijo, and Y. Shigesato, *Thin Solid Films*, **445**, 219 (2003).
25. J. D. Perkins, J. A. del Cueto, J. L. Alleman, C. Warmsingh, B. M. Keyes, L. M. Gedvilas, P. A. Parilla, B. To, D. W. Readey, and D. S. Ginley, *Thin Solid Films*, **411**, 152 (2002).
26. K. J. Saji and M. K. Jayaraj, Thin Solid Films, In press. [DOI:10.1016/j.tsf.2007.10.097].
27. J. Tauc, R. Grigorovici, and A. Vancu, *Phys. Status Solidi*, **15**, 627 (1966).
28. J. Tauc, *Amorphous and Liquid Semiconductors*, J. Tauc, Editor, Plenum, New York (1979).
29. H. Hiramatsu, K. Ueda, H. Ohta, M. Hirano, M. Kikuchi, H. Yanagi, T. Kamiya, and H. Hosono, *Appl. Phys. Lett.*, **91**, 012104 (2007).
30. A. Takagi, K. Nomura, H. Ohta, H. Yanagi, T. Kamiya, M. Hirano, and H. Hosono, *Thin Solid Films*, **486**, 38 (2005).
31. J. F. Wager, D. A. Keszler, and R. E. Presley, *Transparent Electronics*, Chap. 5, Springer-Verlag, New York (2007).
32. C. R. Kagan and P. Andry, *Thin-Film Transistors*, p. 87, Marcel Dekker, New York (2003).
33. K. Nomura, T. Kamiya, H. Ohta, T. Uruga, M. Hirano, and H. Hosono, *Phys. Rev. B*, **75**, 035212 (2007).
34. F. Utsuno, H. Inoue, Y. Shimane, T. Shibuya, K. Yano, K. Inoue, I. Hirosawa, M. Sato, and T. Honma, Thin Solid Films, In press. [DOI: 10106/j.tsf.2007.10.046].
35. T. Kamiya, S. Narushima, H. Mizoguchi, K. Shimizu, K. Ueda, H. Ohta, M. Hirano, and H. Hosono, *Adv. Funct. Mater.*, **15**, 968 (2005).